ELSEVIER

Journal of Fluids and Structures 26 (2010) 253–273

JOURNAL OF FLUIDS AND STRUCTURES

www.elsevier.com/locate/jfs

# Theoretical analysis of hydrostatic implodable cylindrical volumes with solid inner structures

J.J. Cor*, T.F. Miller

*Energy Science and Power Systems Division, Applied Research Laboratory, The Pennsylvania State University, P.O. Box 30, State College, PA 16804, USA*

Received 19 February 2009; accepted 12 September 2009
Available online 2 December 2009

**Abstract**

The basic analytical theory for hydrostatically caused implosions of spherical volumes, which has been known for nearly a century, has been extended for the treatment of cylindrical volumes with deformable solid inner structures. Theoretical analyses are developed that treat the inner structure as infinitely hard, elastically deformable, plastically deformable or shattering under the influence of the pressure from the surrounding implosion event. Parametric studies are made of the effect of the inner structure's geometric and material properties on the pressure field of the surrounding water. Results are compared with a previous study that focused on spherical volumes.


*Keywords:* Potential flow; Underwater implosion

## 1. Introduction

Previously (Cor and Miller, 2009), we explored the implosion of spherical volumes that house spherical inner shells that are infinitely strong, brittle, plastic, or elastic. This work was based on the bubble collapse theory developed by Lord Rayleigh (1917) and Lamb (1932), and subsequently modified by other workers to incorporate the internal gas pressure that permitted the analysis of the oscillating bubble phenomenon. In this theory, the bubble initially contracts under the outside pressure of the liquid. When the interior gas pressure increases to the point where it balances the combined hydrostatic and hydrodynamic heads, the gas volume stops decreasing. Then the higher relative interior pressure acts to force the gas bubble radius outward, until the exterior hydrostatic pressure is enough to counter the interior gas pressure plus the gas hydrodynamic head. The bubble motion reverses itself once again, and the bubble begins to contract. The gas volume oscillation also produces oscillations in the pressure field of the surrounding seawater. The oscillating pressure field can serve as an acoustic source, or if sufficiently large, can produce a pressure wave with sufficient energy to damage nearby structures.

An implodable volume can be defined as any pressure housing containing a non-compensated compressible volume of gas at a pressure below the external sea pressure, which has the potential to collapse. Fluid–structural interactions have been studied previously in related applications. The interaction of an external explosion with a deformable or collapsible inner structure was investigated by Iakovlev (2004, 2006). The interaction of a bubble caused by an

*Corresponding author. Tel.: +1 814 865 6469; fax: +1 814 863 7842.
*E-mail address:* jjc19@psu.edu (J.J. Cor)

0889-9746/$ - see front matter © 2009 Elsevier Ltd. All rights reserved.
doi:10.1016/j.jfluidstructs.2009.09.005

**Nomenclature**

| | |
|---|---|
| $A$ | surface area ($m^2$) |
| $c$ | speed of sound (m/s) |
| $C$ | circumference (m) |
| $E$ | bulk modulus of elasticity (Pa) |
| $F$ | Bernoulli equation function ($m^2/s^2$) |
| $K$ | bulk modulus of plasticity (Pa) |
| $p$ | pressure (Pa) |
| $P$ | gas (acoustic) pressure (Pa) |
| $q$ | kinetic energy ($m^2/s^2$) |
| $r$ | radius (m) |
| $R$ | implodable volume outer radius (m) |
| $t$ | time (s), thickness (m) |
| $U$ | velocity (m/s) |
| $v$ | solid velocity or local velocity (m/s) |
| $V$ | volume ($m^3$) |
| $w$ | potential energy (J) |
| $\gamma$ | ratio of specific heats |
| $\delta$ | differential distance (m) |
| $\varepsilon$ | strain |
| $\mu$ | dynamic viscosity (N s/$m^2$) |
| $\rho$ | density (kg/$m^3$) |
| $\sigma$ | stress (Pa) |
| $\varphi$ | stream function |

*Subscripts*

| | |
|---|---|
| $a$ | acoustic |
| EQ | equilibrium |
| $g$ | gas |
| $H$ | hoop |
| $L$ | liquid or longitudinal |
| LIM | limiting value |
| $m$ | metal |
| 0 | initial condition |
| $r$ | radial |
| $V$ | value at shell inner surface |
| $\infty$Z | far field (infinity) |
| $\theta$ | azimuthal |

underwater explosion with an object on the water surface was studied by Zong (2005) and Klaseboer et al. (2005). Kalumuck et al. (1995) studied bubble interaction with nearby bodies using three-dimensional boundary-element based computer codes. The analysis of real world geometries in studies such as these requires substantial computational resources; however, the objective of this study – as was the objective of our study of spherical structures – is more modest: evaluating the effect of internal structure on the behavior of cylindrical implodable volumes. As previously discussed (Cor and Miller, 2009), the US Navy employs extremely conservative safety factors for controllable volumes, because *subtracting the volume of items internal to the implodable is not allowed*. Therefore, the goal of the current effort is to eventually assess the degree of conservatism of the current safety criteria.

In our previous paper, we gave an overview of the reason for interest in this area as it relates to implodable volumes that might be formed external to submerged vessels, and might cause a safety hazard to those vessels. While implodable volumes with cylindrical geometries are of practical interest in this regard, no cylindrical analog exists for the Rayleigh collapse model. Kedrinskii (1976) proposed an approximation compatible with experimental data that also is supported by studies for supercavitating flows. Kedrinskii's approach has been used to predict the implosion of cylindrical volumes that house cylindrical inner shells that are infinitely strong, brittle, plastic, or elastic; see Fig. 1.

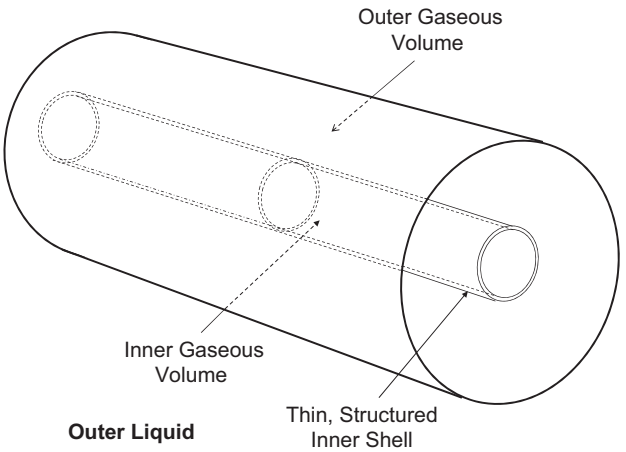


Fig. 1. Implodable volumes with cylindrical geometry.

## 2. Basic theory—cylindrical volume with infinitely strong inner structure

Starting with the assumption of an irrotational and incompressible external fluid, its movement can be described with the Bernoulli Eq.

$$\frac{\partial\phi}{\partial t} - q + F(t) = \frac{p}{\rho}, \tag{1}$$

where $\varphi$ is the velocity potential, $q$ the kinetic energy, $p$ the liquid pressure, $\rho$ the liquid density and $F(t)$ is a function of time. For the case of spherical coordinates, the velocity potential satisfies Poisson's Eq.

$$\frac{\partial}{\partial r}\left(r^2\frac{\partial\phi}{\partial r}\right) = 0. \tag{2}$$

The Bernoulli equation and Poisson's equation lead, with some manipulation, to the equation of motion of an imploding spherical volume

$$R\left(\frac{\mathrm{d}^2R}{\mathrm{d}t^2}\right) + \frac{3}{2}\left(\frac{\mathrm{d}R}{\mathrm{d}t}\right)^2 = \frac{1}{\rho}\left\{p_{g_0}\left[\frac{{R_0}^3 - {R_V}^3}{R^3 - {R_V}^3}\right]^{\gamma} - p_\infty\right\}, \tag{3}$$

where $R$ is the radius of the volume, $R_0$ its initial radius, $R_V$ the radius of the inner volume, and $\gamma$ the ratio of specific heats.

Vokurka (1985) showed that the pressure in the liquid surrounding the implodable volume is given by

$$p_a = \frac{R}{r}P_a + \frac{1}{2}\frac{R}{r}\left(\frac{\mathrm{d}R}{\mathrm{d}t}\right)^2 - \frac{1}{2}\left(\frac{R}{r}\right)^4\left(\frac{\mathrm{d}R}{\mathrm{d}t}\right)^2. \tag{4}$$

In Eq. (4), $p_a$ refers to the acoustic (local minus hydrostatic) pressure and $P_a$ refers to the acoustic pressure of the gas. The basis of our previous work (Cor and Miller, 2009) was the solution of Eqs. (3) and (4) using the Runge–Kutta–Nystrom method with a time step in the order of $10^{-7}$ s.

An exact analytical solution does not exist for cylindrical geometries, because the Bernoulli equation is unbounded at infinity. Therefore, our previous study was centered on spherical geometries. However, Kedrinskii (2005) proposed using an approximate conservation law for flow in cylindrical geometries based on the Kirkwood–Bethe hypothesis (Cole, 1948)

$$r\left(1 - \frac{v}{c}\right)\frac{\mathrm{d}v}{\mathrm{d}t} + \frac{3}{4}\left(1 - \frac{v}{3c}\right)v^2 = \frac{1}{2}\left(1 + \frac{v}{c}\right)w + \frac{r}{c}\left(1 - \frac{v}{c}\right)\frac{\mathrm{d}w}{\mathrm{d}t}. \tag{5}$$

In Eq. (5), $c$ is the local speed of sound, $v$ is the local velocity and $w = \int_{p_\infty}^{p} \mathrm{d}p/\rho$. If the speed of sound is infinite, as it is in an incompressible fluid, Eq. (5) becomes

$$r\frac{\mathrm{d}v}{\mathrm{d}t} + \frac{3}{4}v^2 = \frac{1}{2}\frac{p - p_\infty}{\rho}. \tag{6}$$

For cylindrical symmetry,

$$v = \frac{R}{r}\frac{\mathrm{d}R}{\mathrm{d}t} \tag{7}$$

Substituting Eq. (7) into Eq. (6), along with the definition of a total derivative,

$$\frac{\mathrm{d}v}{\mathrm{d}t} = \frac{\partial v}{\partial t} + v\frac{\partial v}{\partial r}, \tag{8}$$

yields the following:

$$2\left(R\frac{\mathrm{d}^2R}{\mathrm{d}t^2}+\left(\frac{\mathrm{d}R}{\mathrm{d}t}\right)^2\right)-\frac{1}{2}\frac{R^2}{r^2}\left(\frac{\mathrm{d}R}{\mathrm{d}t}\right)^2=\frac{p-p_\infty}{\rho}. \tag{9}$$

At the surface of the bubble, assuming the ideal gas law, this becomes

$$2\left[R\frac{\mathrm{d}^2R}{\mathrm{d}t^2}+\left(\frac{\mathrm{d}R}{\mathrm{d}t}\right)^2\right]-\frac{1}{2}\left(\frac{\mathrm{d}R}{\mathrm{d}t}\right)^2=\frac{1}{\rho}\left\{p_{g_0}\left[\frac{{R_0}^2-{R_V}^2}{R^2-{R_V}^2}\right]^\gamma-p_\infty\right\}. \tag{10}$$

However, applying Eq. (9) far from the bubble surface leads to physically unrealistic results.

It is also possible to integrate Euler's equation in cylindrical coordinates to produce the following equation for motion in the liquid

$$\frac{p-p_\infty}{\rho}=\left[\left(\frac{\mathrm{d}R}{\mathrm{d}t}\right)^2+R\frac{\mathrm{d}^2R}{\mathrm{d}t^2}\right]\ln\left(\frac{{R_{\mathrm{LIM}}}^2}{r^2}\right)+\frac{1}{2}\left[\frac{R^2}{{R_{\mathrm{LIM}}}^2}-\frac{R^2}{r^2}\right]\left(\frac{\mathrm{d}R}{\mathrm{d}t}\right)^2, \tag{11}$$

where $R_{\mathrm{LIM}}$ is a limiting value of fluid radius beyond which the bubble does not entrain mass. Kedrinskii (1976) assigned a value $r_0$ to this radius when the bubble radius is $R_0$. Eq. (11) can then be re-written as

$$\frac{p-p_\infty}{\rho}=\left[\left(\frac{\mathrm{d}R}{\mathrm{d}t}\right)^2+R\frac{\mathrm{d}^2R}{\mathrm{d}t^2}\right]\ln\left(\frac{r_0^2-R_0^2+R^2}{r^2}\right)+\frac{1}{2}\left[\frac{R^2}{r_0^2-R_0^2+R^2}-\frac{R^2}{r^2}\right]\left(\frac{\mathrm{d}R}{\mathrm{d}t}\right)^2. \tag{12}$$

Through comparison of Eq. (12) with experimental data, Kedrinskii indicated that good agreement was observed when the approximation $\ln(r_0/R)\approx 2$ was made. Likhterov (2000) employed this approximation to the study of high-frequency acoustic emission generated by a cylindrical underwater explosion. Serebryakov (1976) and Logvinovich and Serebryakov (1975) developed equations identical in form for the prediction of the cylindrically symmetric shape for a supercavitating bubble in high speed flows. Their work presented a theoretical and mathematical basis for setting $\ln(r_0/R)=2$. Good agreement between simulations made using these equations and observations of supercavitating bubbles (Logvinovich, 1969) gives additional support for the approximation. In addition, making this approximation, along with the approximation that $r_0>>R$, reduces Eq. (12) to the same form as Eq. (10) at the bubble surface.

Eq. (12) can be re-arranged to calculate the acoustic pressure

$$p_a=\rho\left[\left(\frac{\mathrm{d}R}{\mathrm{d}t}\right)^2+R\frac{\mathrm{d}^2R}{\mathrm{d}t^2}\right]\ln\left(\frac{r_0^2-R_0^2+R^2}{r^2}\right)+\frac{1}{2}\left[\frac{R^2}{r_0^2-R_0^2+R^2}-\frac{R^2}{r^2}\right]\left(\frac{\mathrm{d}R}{\mathrm{d}t}\right)^2. \tag{13}$$

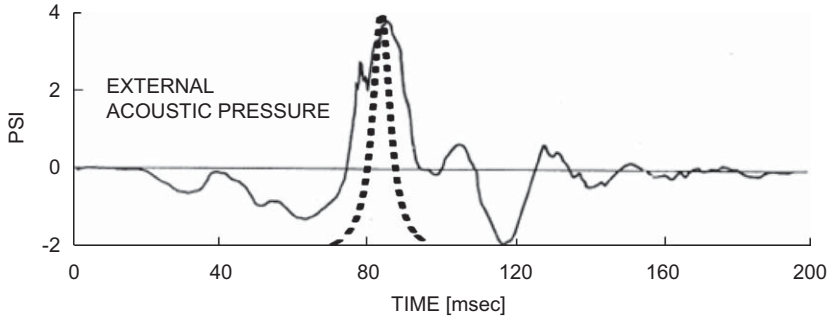


Fig. 2. Comparison of measured acoustic signal from the implosion of a 30-inch-diameter cylinder measured by Price and Shuler (solid line) with the calculated acoustic response (dotted line).

Table 1
Sample analysis problem conditions.

| | |
|---|---|
| Initial radius | 50 cm |
| Strong inner shell radius | 5 cm |
| Initial shell pressure | 1 atm |
| Time increment of calculations | $10^{-7}$ s |
| Depth | 100 m |
| Liquid medium | Water |
| Gas medium | Air |

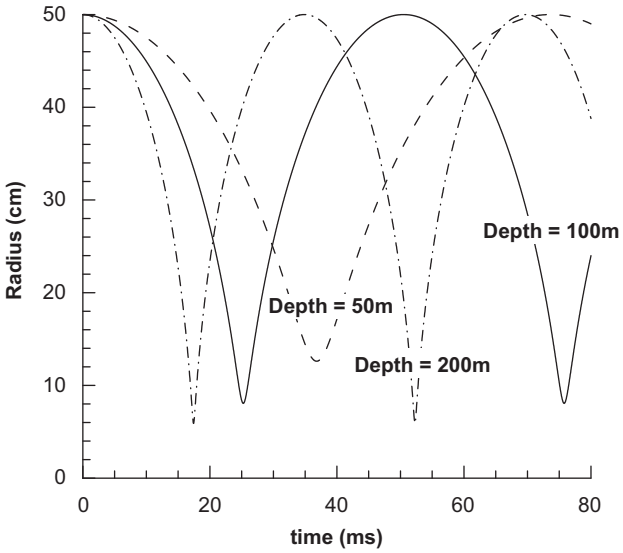


Fig. 3. Cylindrical volume radius under conditions given in Table 1. Dashed lines present results for depth variations from the baseline value of 100 m.

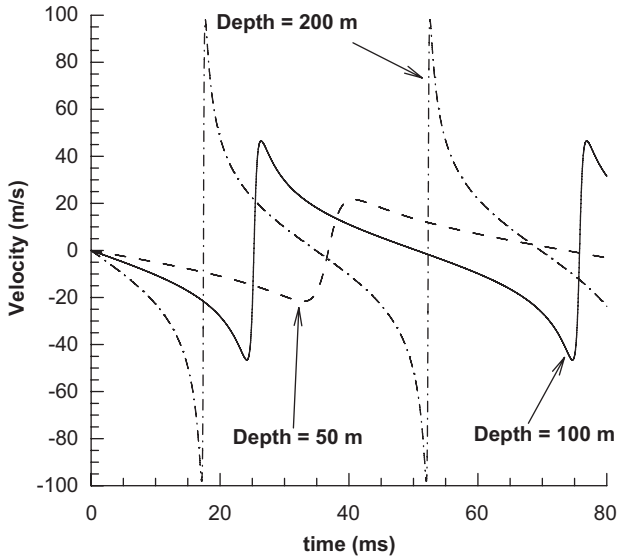


Fig. 4. Cylindrical volume surface velocity under the conditions given in Table 1. Dashed lines present results for depth variations from the baseline value of 100 m.

On the bubble surface, Eq. (12) becomes

$$\left[\left(\frac{\mathrm{d}R}{\mathrm{d}t}\right)^2 + R\frac{\mathrm{d}^2R}{\mathrm{d}t^2}\right]\ln\left(\frac{r_0^2 - R_0^2 + R^2}{R^2}\right) + \frac{1}{2}\left[\frac{R^2}{r_0^2 - R_0^2 + R^2} - 1\right]\left(\frac{\mathrm{d}R}{\mathrm{d}t}\right)^2 = \frac{1}{\rho}\left\{p_{g_0}\left[\frac{{R_0}^2 - {R_V}^2}{R^2 - {R_V}^2}\right]^{\gamma} - p_\infty\right\}. \tag{14}$$

In the work reported below, Eq. (14) was integrated numerically using the Runge–Kutta–Nystrom method with a time step in the order of $10^{-7}$ s. At each time step, the values for $R$, $\mathrm{d}R/\mathrm{d}t$ and $\mathrm{d}^2R/\mathrm{d}t^2$ obtained from integrating Eq. (14) were inserted into Eq. (13) to obtain the acoustic pressure in the surrounding liquid.

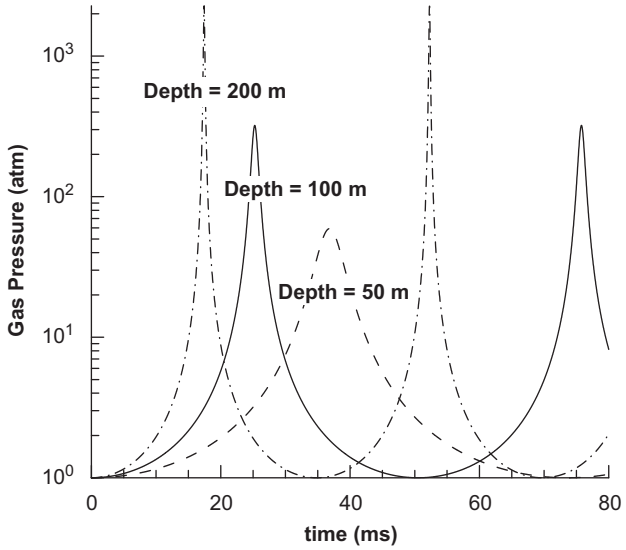


Fig. 5. Cylindrical volume gas pressure under conditions given in Table 1. Dashed lines present results for depth variations from the baseline value of 100 m.

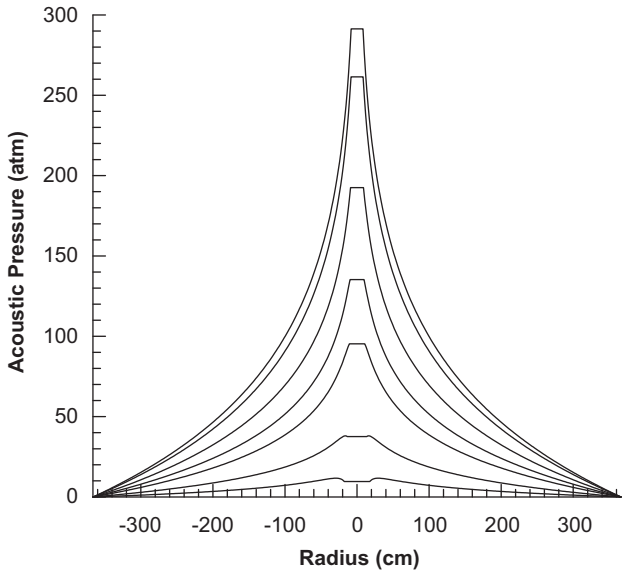


Fig. 6. Acoustic pressure in liquid surrounding cylindrical volume under conditions given in Table 1. In the order of increasing magnitude, the data are presented at 22.8, 23.8, 24.4, 24.6, 24.8, 25.0, and 25.4 ms (peak magnitude of acoustic field).

A comparison was made between the predictions of Eqs. (13) and (14) and experimental data from a study by Price and Shuler (1974). In this study, cylinders were lowered or dropped into the ocean and sank until they imploded. Hydrophones recorded the acoustic signals from the imploding cylinders. Fig. 2 shows hydrophone data for a 0.76 m diameter by 2.44 m long carbon-steel cylinder tank that was lowered into the water and whose implosion was estimated to occur at a depth of 40 m. Also shown in this figure is the calculated acoustic response from the cavity implosion. The location of the hydrophone relative to the tank at the time of implosion was not given, so calculated results are normalized to the peak acoustic intensity. The modeling appears to capture to fundamental harmonic of the structural implosion to an encouraging degree, considering the approximate nature of the experimental reporting.

An example analysis was made of an implodable cylindrical volume under the conditions given in Table 1. Fig. 3 shows the calculated radius for the volume through the first cycle of oscillation. The volume reaches its minimum and returns to its initial value in approximately 52 ms, after which the cycle repeats itself. Also shown in Fig. 3 are results where the volume depth is half and twice the baseline depth of 100 m. The effect of increasing depth is to decrease both the period of oscillation and the minimum radius of the gas volume. Fig. 4 shows the velocity of the volume's outer surface for the baseline depth and half and twice the baseline depth. The peak surface velocities increase with depth. Fig. 5 shows how the interior gas pressure varies with time. As expected, the peak pressure increases with depth. Figs 3–5 show that the minimum radius, peak velocity and peak pressure all occur at the same point. Fig. 6 presents a sequence of values of the liquid acoustic pressure, up to the peak pressure, calculated using Eq. (13). The range of influence for the imploding volume is limited by the $\ln(r_0/R) \approx 2$ assumption; however, we are interested in only the initial pressure pulse in close proximity.

## 3. Inner shell deformation or failure

### 3.1. Stress analysis

Study cases were chosen such that the inner shell was allowed to fracture in a brittle fashion, or deform plastically or elastically. The analyses were made with the assumption that the inner, solid structure responds instantaneously to disturbances. For all cases the thin-walled assumption was made for computing inner shell stresses. For shells with thickness less than one-tenth the inner wall radius, this assumption results in errors of less than 5% of the actual wall stress. For a thin-walled cylindrical vessel, the longitudinal (axial) and hoop stresses are given by

$$\sigma_L = \frac{1}{2}(p_{\text{inner}} - p_{\text{outer}})\frac{r}{t}, \quad \sigma_H = (p_{\text{inner}} - p_{\text{outer}})\frac{r}{t}, \tag{15}$$

where $t$ is the thickness of the vessel wall, the outer pressure is that of the imploding volume surrounding the inner shell, and the inner pressure is the pressure of gas volume contained by the inner shell. The inner and outer pressures are transient, and therefore the stress acting on the shell is transient as well. The propagation of stress through the elastic/plastic/brittle shells was assumed to occur infinitely fast. The wall stresses are principal stresses and it was assumed that failure occurs in one of the shell's principal planes.

### 3.2. Brittle shell

For the case of a brittle shell, when the principal stress exceeded the maximum allowable stress, the shell was assumed to shatter. Such an assumption might be appropriate for a cast iron or composite material, for instance. It was assumed that the shell retains its initial thickness and radius up to the point where the maximum allowable stress is reached. When the maximum

Table 2
Sample brittle inner shell problem conditions.

| | |
|---|---|
| Initial gas volume radius | 50 cm |
| Brittle shell outer radius | 40 cm |
| Brittle shell thickness | 5 mm |
| Initial gas pressure | 1 atm |
| Time increment of calculations | $10^{-7}$ s |
| Gas volume depth | 100 m |
| Liquid medium | Water |
| Gas medium | Air |
| Shell failure stress | 0.33 GPa |

allowable stress was reached, the shell shattered, and Eqs. (13) and (14) were re-adjusted by re-setting the shell radius $R_V$ to zero, and re-setting $R_0$ to the value of $R$ at the point of failure. The gas pressure at the point of shattering was calculated by assuming that the gas in the inner shell, at $p_{\text{inner}}$, and the gas in the surrounding volume, at $p_{\text{gas}}$, mix isentropically

$$p_{\text{new}} = p_{\text{inner}}\left(\frac{R_V}{R}\right)^2 + p_{\text{gas}}\left[1 - \left(\frac{R_V}{R}\right)^2\right]. \tag{16}$$

$R_V$ in Eq. (16) is the radius of the inner shell before failure. The isentropic mixing assumption is one limiting case of conditions inside the gas volume at the point of shell failure. The study of non-isentropic mixing of the two gases was

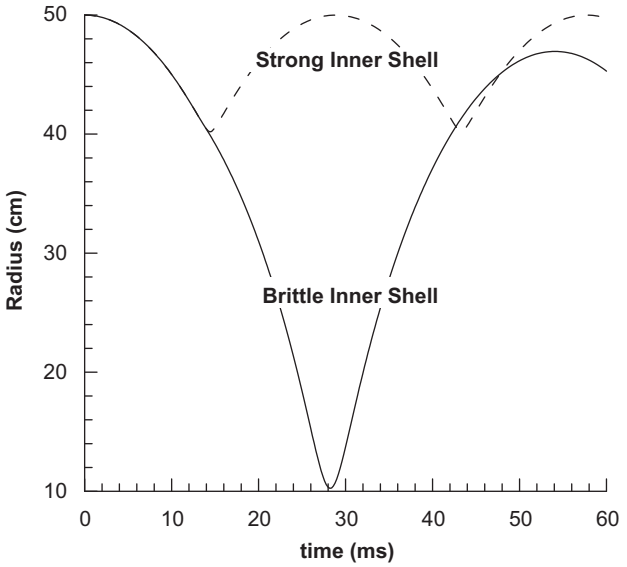


Fig. 7. Cylindrical volume radius under conditions given in Table 2, assuming a strong inner shell (dashed line) and a brittle inner shell (solid line).

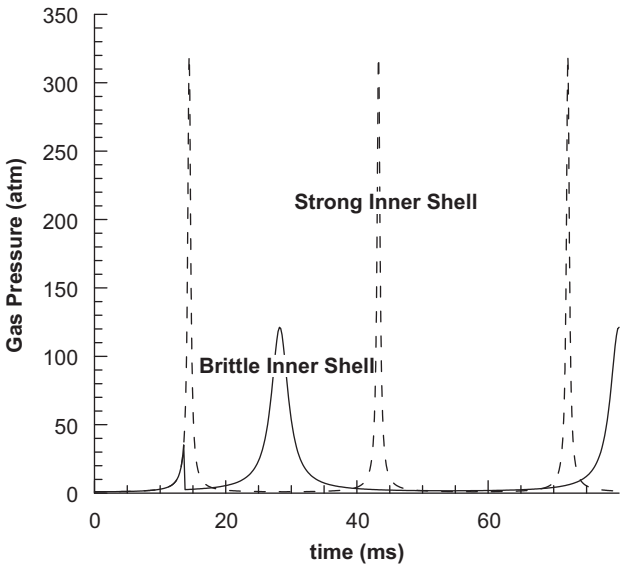


Fig. 8. Cylindrical volume gas pressure under conditions given in Table 2, assuming a strong inner shell (dashed line) and a brittle inner shell (solid line).

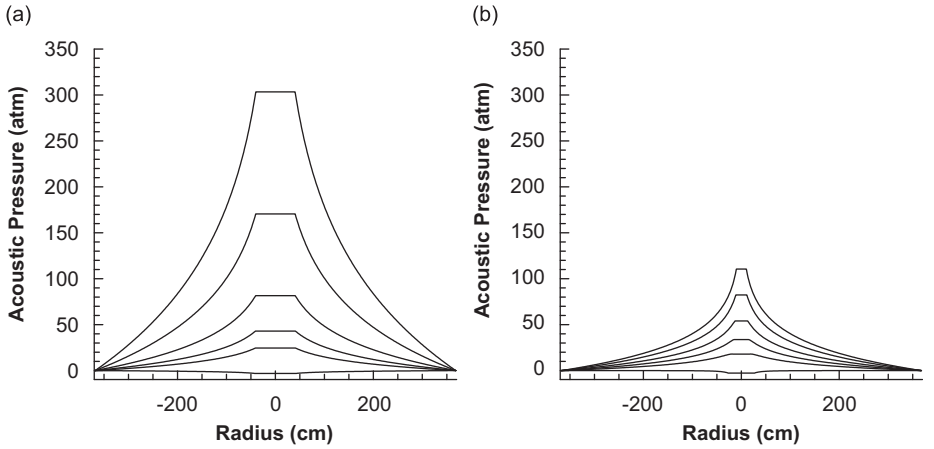


Fig. 9. Acoustic pressure in liquid surrounding cylindrical volume under conditions given in Table 2, assuming an infinitely strong inner shell (a) and brittle inner shell (b). In the order of increasing magnitude, the data for Fig. 9 (a) are presented at 12.2, 13.6, 13.8, 14.0, 14.2, and 14.4 ms (the time of peak magnitude of the acoustic field). In the order of increasing magnitude, the data for Fig. 9 (b) are presented at 21.8, 25.4, 26.2, 26.8, 27.4, and 28.2 ms (the time of peak magnitude of the acoustic field).

left as a venue for future research. Isentropic mixing and compression of the gas is the most conservative assumption. Propagation of a gas phase shock wave will act to dissipate some of the implosion energy, as will any form of two-phase mixing. The reflected pressure impulse with high theoretical levels predicted can only occur if the structure fails uniformly and the compression process is independent of azimuth.

An example problem with a brittle shell was run using the conditions shown in Table 2. The failure stress was chosen to be consistent with cast iron. To make a more ready comparison with results for spherical geometries, the values in this table are the same as used in Cor and Miller (2009).

The analysis was first run assuming an infinitely strong inner shell that was not allowed to fail, and then was run assuming the shell is brittle. With the brittle shell, failure occurred at 14 ms at a gas pressure of 42 atm. Fig. 7 shows the calculated gas radius for the strong and brittle cases. The failure of the shell reduces the minimum gas radius and increases the period of oscillation. Fig. 8 shows a plot of the gas pressure assuming a strong and brittle inner shell. The effect of shell failure is to reduce the peak gas pressure by almost a factor of three. The same reduction in the water's acoustic pressure can be seen by comparing Figs. 9(a) and (b). The times in Fig. 9(b) are centered on the peak acoustic pressure, which can be identified by the second peak in Fig. 8.

### 3.3. Plastic shell

A dynamic model for the plastic deformation of casings under external loads was developed by Tan et al. (2003). They used the following constitutive law for viscoplastic (ignoring elastic) deformation:

$$\sigma_\theta - \sigma_r = \mathrm{sgn}\left(\frac{\mathrm{d}r_2}{\mathrm{d}t}\right)2K - 4\mu\left(\frac{\mathrm{d}v}{\mathrm{d}r}\right), \tag{17}$$

where $\sigma_\theta$ is the azimuthal stress, $\sigma_r$ the radial stress, $\mathrm{d}r_2/\mathrm{d}t$ the velocity on the outer surface of the casing, $\mu$ the dynamic viscosity, $v$ the radial velocity in the casing, sgn the sign function, and $K$ the bulk modulus of plasticity. They also expressed the conservation of mass and Euler's equation as

$$\frac{\mathrm{d}v}{\mathrm{d}r} + N\frac{v}{r} = 0, \tag{18}$$

and

$$\rho_m\left(\frac{\mathrm{d}v}{\mathrm{d}t} + v\frac{\mathrm{d}v}{\mathrm{d}r}\right) = \frac{\mathrm{d}\sigma_r}{\mathrm{d}r} + \frac{N}{r}(\sigma_r - \sigma_\theta), \tag{19}$$

where $N = 1$ for cylindrical geometries and $N = 2$ for spherical geometries, and $\rho_m$ is the density in the casing.

Combining Eqs. (17), (18), and (19), it can be shown that the equation of motion for the cylindrical casing is

$$\rho_m \ln\left(\frac{r_2}{r_1}\right)\frac{d^2 r_1}{dt^2} + \rho_m\left[\ln\left(\frac{r_2}{r_1}\right) - \frac{1}{2}\left(1-\left(\frac{r_2}{r_1}\right)^2\right)\right]\left(\frac{dr_1}{dt}\right)^2 = \sigma_r(r_2) - \sigma_r(r_1) - \mathrm{sgn}\left(\frac{dr_2}{dt}\right)2K\ln\left(\frac{r_2}{r_1}\right) - \frac{2\mu}{r_1}\left[1-\left(\frac{r_2}{r_1}\right)^2\right]\frac{dr_1}{dt}, \tag{20}$$

where $r_2$ is the outer casing radius and $r_1$ the inner casing radius. For the current application, $\sigma_r(r_2)$ is the negative of the gas pressure of the implodable volume and $\sigma_r(r_1)$ is the negative of the gas pressure inside the shell, which now varies as the shell expands or contracts based on the ideal gas law. As the implodable volume's expansion and contraction was calculated, Eq. (20) was integrated, using the Runge–Kutta–Nystrom method, to obtain the inner radius of the plastic shell as a function of time. Assuming the shell material is incompressible, mass conservation was used to calculate the outer shell radius from the updated value of the inner shell radius. This relatively simple numerical integration of Eq. (20) was used in lieu for doing a complete FEM analysis of the shell, which was deemed a reasonable approximation for the thin shells analyzed in this study.

An example problem was run using the conditions listed in Table 3. Again, the values are the same as used by Cor and Miller (2009). Shell material properties were taken from those reported by Tan et al. (2003). To isolate the effect of plastic deformation, the shell was not allowed to fail, although stresses would be great enough to have done so. Fig. 10 shows the trace of the gaseous volume's radius versus time when the inner shell is infinitely strong, and when it is plastic. Fig. 11 shows the corresponding gas pressures for the infinitely strong and plastic shells. The scale in Fig. 11 was changed to logarithmic to better display the pressure traces on the same graph. It can be seen that the plastic deformation of the shell reduces the maximum gas pressure inside the implodable volume by almost two orders of magnitude. Fig. 12 shows the variation of the plastic shell's outer radius with time. After the outer gas pressure reaches a critical level, the shell plastically deforms to a new radius. It can be seen that the change in radius goes through three brief periods of zero slope. These points of zero slope come about because as the inner shell contracts, an increase in the gas volume ensues. The pressure in the outer gas volume decreases, temporarily halting further compression of the inner shell. Pressure must build up once again to a point where compression of the inner shell can continue. A comparison of the liquid acoustic pressure fields assuming a strong and plastic shell is presented in Fig. 13. The results show that the plastic deformation of the shell reduces acoustic pressure excursions by two orders of magnitude.

### 3.4. Elastic shell

For elastic materials, the assumption was made that the stress propagation is instantaneous. This again allows for a simplified analysis of the shell. For a purely elastic thin shell, the average azimuthal strain is

$$\varepsilon = \frac{\sigma_\theta}{E}, \tag{21}$$

where $E$ is the bulk modulus of elasticity. The azimuthal strain is the same as the hoop stress, calculated in Eq. (15), and changes in value as the structure's inner pressure and outer (gas volume surrounding the structure) pressure change. The

Table 3
Sample plastic inner shell problem conditions.

| | |
|---|---|
| Initial gas volume radius | 100 cm |
| Shell outer radius | 88 cm |
| Shell thickness | 8 mm |
| Initial gas pressure | 1 atm |
| Initial inner shell pressure | 1 atm |
| Time increment of calculations | $10^{-7}$ s |
| Gas volume depth | 300 m |
| Liquid medium | Water |
| Gas medium | Air |
| Material viscosity | 3000 N s/m$^2$ |
| Material density | 7890 kg/m$^3$ |
| Plasticity modulus | 0.53 GPa |
| Modulus of elasticity* | 8 GPa |

*Used for elastic shell analysis.

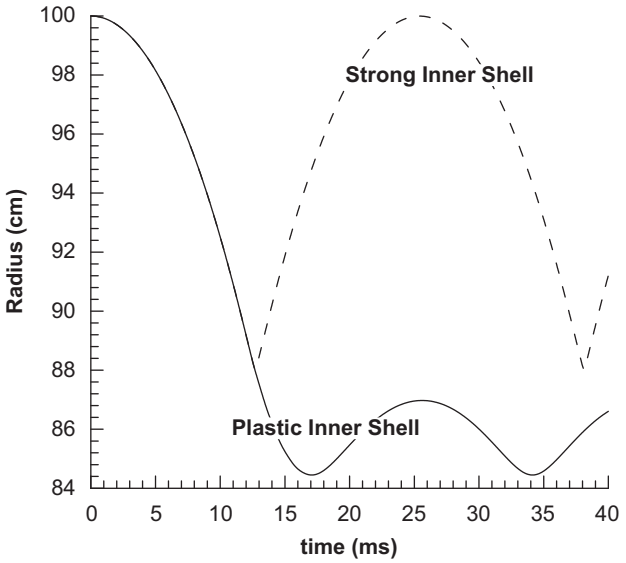


Fig. 10. Outer gas volume radius under conditions given in Table 3, assuming a strong inner shell (dashed line) and a plastic inner shell (solid line).

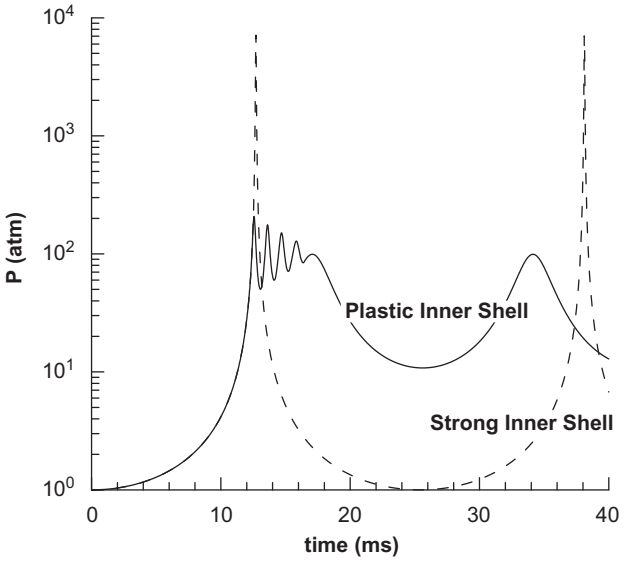


Fig. 11. Outer gas volume pressure under conditions given in Table 3, assuming a strong inner shell (dashed line) and a plastic inner shell (solid line).

differential change of circumference ($\delta C$) is found from

$$\delta C = C\varepsilon = \frac{2\pi r\sigma_\theta}{E}. \tag{22}$$

The change in radius is then

$$\delta r = \frac{\delta C}{2\pi} = \frac{r\sigma_\theta}{E}. \tag{23}$$

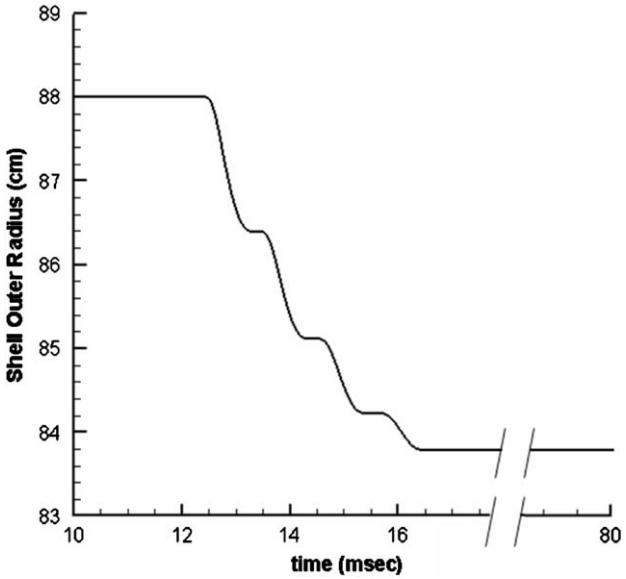


Fig. 12. Inner shell's outer radius under conditions given in Table 3, assuming that the inner shell deforms plastically.

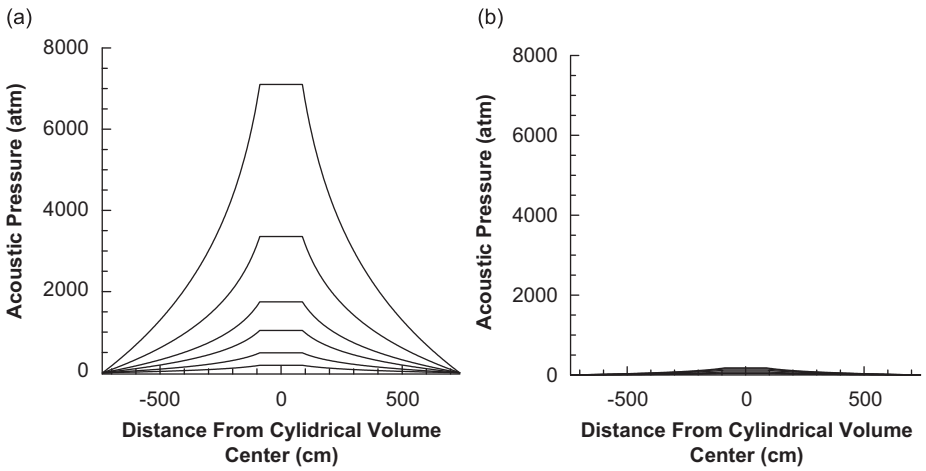


Fig. 13. Acoustic pressure in liquid surrounding cylindrical volume under conditions given in Table 3, assuming that the inner shell does not fail or deform (a) and assuming that the inner shell deforms plastically (b). In the order of increasing magnitude, the data in Fig. 13 (a) are presented at 12.51, 12.59, 12.63, 12.65, 12.67, and 12.71 ms (the time of peak magnitude of the acoustic field). In the order of increasing magnitude, the data in Fig. 13 (b) are presented at 12.29, 12.35, 12.41, 12.47, 12.51, and 12.57 ms (the time of peak magnitude of the acoustic field).

In terms of the inner shell radius ($r_1$) the inner shell strain is

$$\varepsilon_1 = \frac{\delta r_1}{r_1} = \frac{\sigma_\theta}{E}. \tag{24}$$

If the shell material is incompressible, the outer shell strain must then be (neglecting higher order terms)

$$\varepsilon_2 = \varepsilon_1 \left(\frac{r_1}{r_2}\right)^2. \tag{25}$$

Updated inner and outer radii are then given by

$$r_1(\text{new}) = r_1(1+\varepsilon_1), \quad r_2(\text{new}) = r_2(1+\varepsilon_2). \tag{26}$$

At each time step in the integration of the problem, the strains $\varepsilon_1$ and $\varepsilon_2$ were calculated using Eqs. (15), (24) and (25), and new inner structure inner and outer radii were calculated using Eq. (26). These new radii were then used in the succeeding time step of the integration. The inner shell pressure was updated based on its shell radius using the ideal gas law. This relatively simple analysis was again used in lieu of complete FEM analysis of stress and strain in the shell.

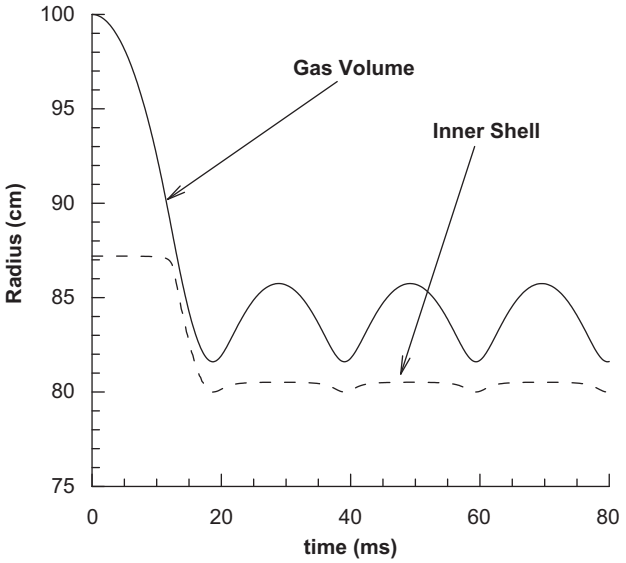


Fig. 14. Cylindrical gas volume radius (solid line) and shell outer radius (dashed line) under conditions given in Table 3, assuming that the inner shell deforms elastically.

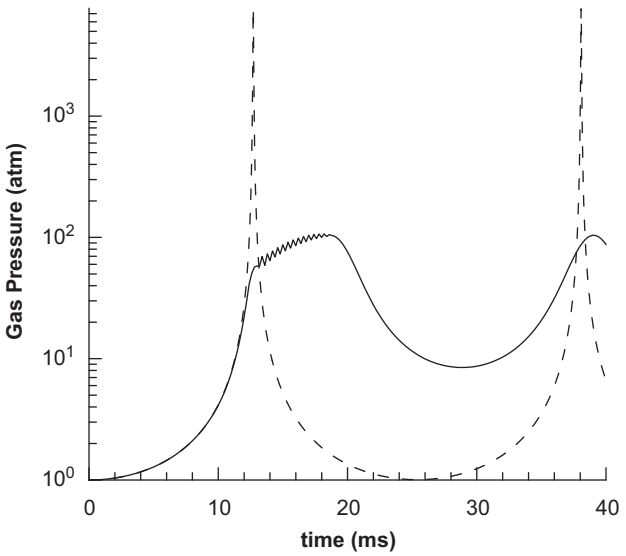


Fig. 15. Outer volume gas pressure under conditions given in Table 3, assuming a strong inner shell (dashed line) and an elastic inner shell (solid line).

An example analysis for an elastic shell was run under the conditions given in Table 3. The modulus of elasticity chosen was that of cast iron. The shell was not allowed to fail so that the effect of the elastic deformation could be isolated. Fig. 14 shows the variation of the gaseous volume's radius and the shell's outer radius with time. The gaseous radius behaves in a manner similar to that found for the plastic shell (Fig. 10), although in Fig. 14 it assumes a smaller minimum radius in its oscillations. This is because the shell radius reaches a smaller minimum value than it did in the plastic case (Fig. 12). The elastic shell oscillates about a new, lower value after an initial contraction. Fig. 15 shows the variation of the outer volume's gas pressure with time assuming an elastic inner shell, with the pressure trace for the strong inner shell included for reference. There is an oscillation in the gas pressure during the first contraction of the elastic shell, although at a higher frequency than encountered for the plastic case (Fig. 11).

Fig. 16 shows the calculated liquid acoustic pressure for the case of an elastic inner shell. The scale of this figure was expanded relative to Fig. 13 so that the pressure excursions could be displayed in detail. The acoustic excursions are significantly reduced over those found assuming an infinitely strong inner shell (Fig. 13 (a)) and the plastic inner shell (Fig. 13 (b)). This is not surprising when the peak gas pressure for the elastic shell (Fig. 15) is compared to the peak pressure shown for the plastic shell (Fig. 11).

The results of the analysis of deformable cylindrical shells are similar to the analytical results for deformable spherical shells. They indicate that there is some non-recoverable work that is done in compressing the shell to a new equilibrium value. This is true whether the shell deforms elastically or plastically. The equations for the gas may have to be modified to accurately calculate the additional pressure losses due to this non-recoverable work.

### 3.5. *Failure of deformable shells*

The analysis of the plastic and elastic shells was now modified so that they would both fail at the failure stress value given in Table 2. Failure of the plastic shell occurred at 12.04 ms at a pressure of 30.74 atm. Failure of the elastic shell occurred at 12.21 ms at a pressure of 30.98 atm. At this point, the shell was assumed to have shattered and results were similar for the two cases.

Fig. 17 is a plot of the gaseous volume radius and pressure for the cases where the shells failed. The maximum pressure in Fig. 17 is one order of magnitude higher than shown in Figs. 11 and 15 for the plastic and elastic shells. The work that was done to compress the shells plastically or elastically is now available for compression of the gas volume, and the pressure in the gas is therefore higher.

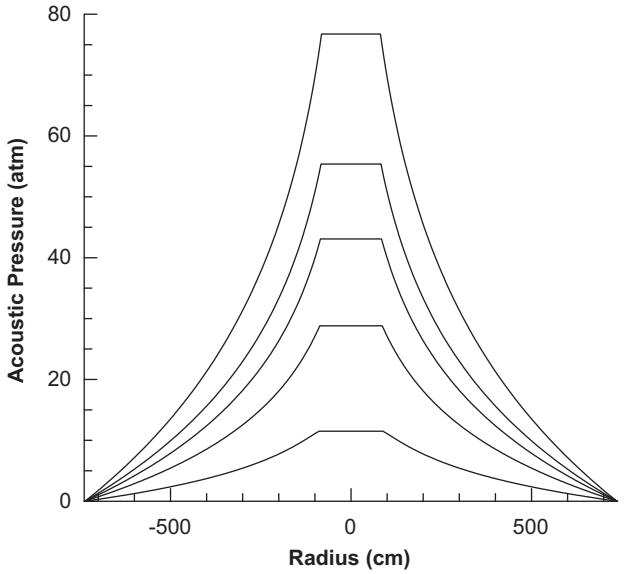


Fig. 16. Acoustic pressure in liquid surrounding cylindrical volume under conditions given in Table 3, assuming that the inner shell deforms elastically. In the order of increasing magnitude, the data are presented at 12.39, 13.59, 14.79, 15.99, and 18.19 ms (the time of peak magnitude of the acoustic field).

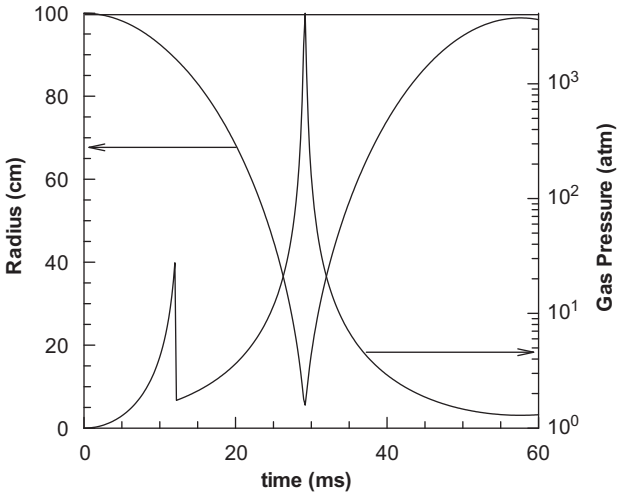


Fig. 17. Outer volume radius and pressure under conditions given in Table 3, when the inner shell (plastic or elastic) fails.

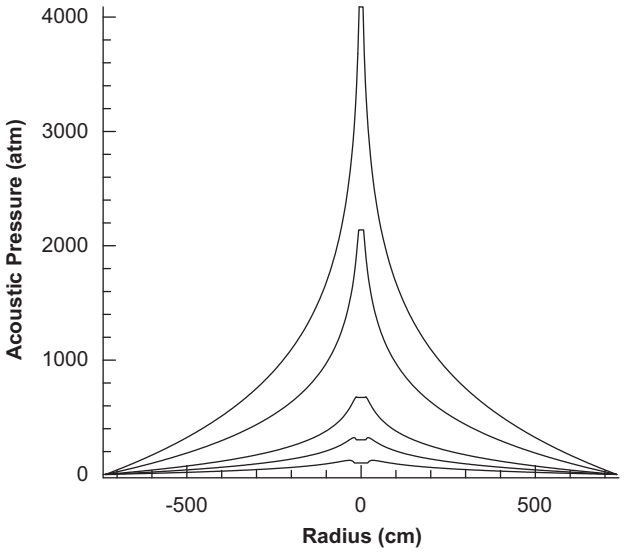


Fig. 18. Acoustic pressure in liquid surrounding cylindrical volume under conditions given in Table 3, when the plastic inner shell (plastic or elastic) fails. In the order of increasing magnitude, the data are presented at 28.19, 28.59, 28.79, 28.99, and 29.19 ms (the time of peak magnitude of the acoustic field).

Fig. 18 shows the acoustic pressure in the surrounding liquid when the shell is allowed to fail. Although the peak acoustic pressure is increased over that of Figs. 13 (b) and 16, it is still significantly reduced over that shown in Fig. 13 (a) for the infinitely strong shell.

## 4. Parametric study

### *4.1. Non-destructible plastic inner shell*

A parametric study was made of implodable volumes with a plastic inner structure over a range of conditions. Studies showed that the structures were relatively insensitive to the values of material viscosity and density chosen, so values of

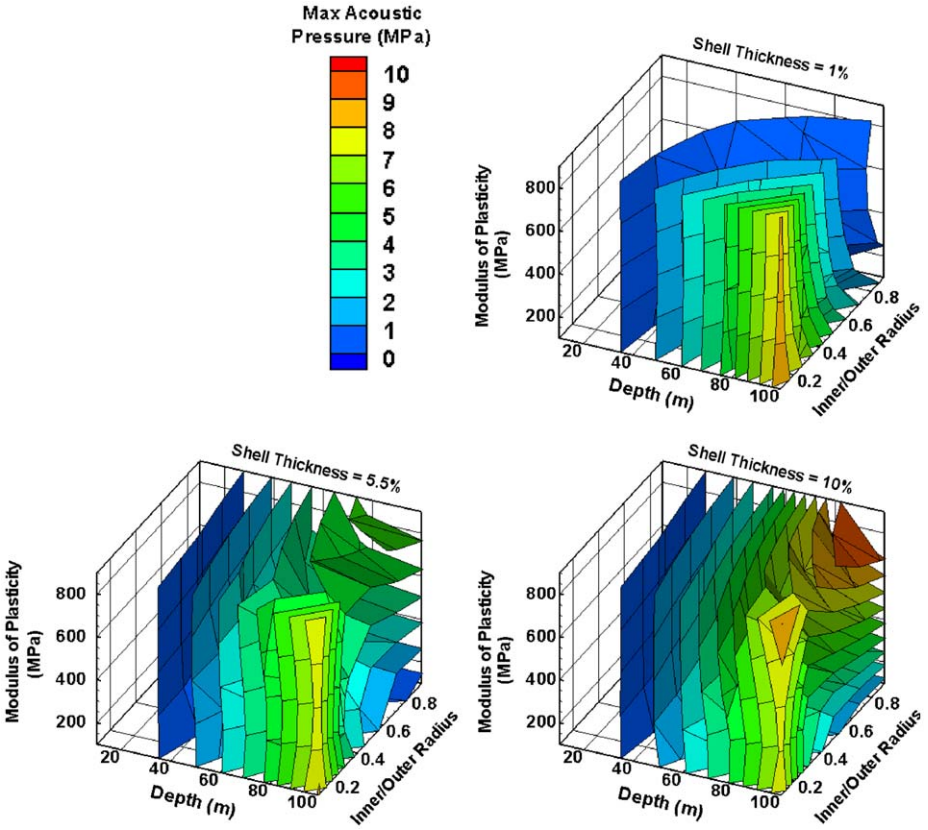


Fig. 19. Contour plots of maximum acoustic pressure at two times the initial outer volume radius with plastic inner shell with an initial outer shell radius of 10 cm.

4000 N s/m$^2$ and 7850 kg/m$^3$ were assigned, respectively. Fig. 19 is a set of contour plots for the maximum acoustic pressure at two initial gas volume radii with an initial outer gas volume radius of 10 cm. The axes of this figure are the depth below the surface, the ratio of the initial inner plastic shell radius to the initial outer gas shell radius, and the material modulus of plasticity. The inner shell thicknesses are reported in percents of the initial plastic shell radius. The maximum acoustic pressure tends to be largest at the maximum depth and the minimum inner-to-outer radius ratio. This is because the gaseous volume being compressed is reduced as the inner radius approaches the value of the outer radius. The maximum acoustic pressure increases with depth because at greater depths the gaseous volume can be compressed to a greater degree. Increasing the modulus of plasticity tends to increase the acoustic pressure. Thicker inner shells increase the maximum acoustic pressure by making the inner structure stronger and allowing more work to go into compression of the gas. At large depths and high values of the plasticity modulus and shell thickness, inner-to-outer radius ''minima'' begin to appear. Below the value of these minima, the increase in the gaseous volume causes the maximum acoustic pressure to increase; above these minima, the increased strength of the shell causes the acoustic pressure to increase.

### 4.2. Non-destructible elastic inner shell

A parametric study was made of implodable volumes with an elastic inner structure over a range of conditions. The maximum acoustic pressure was again calculated at a distance of two times the initial outer gas volume radius. Fig. 20 is a set of contour plots for the maximum acoustic pressure at this distance when the inner shell has an elastic modulus of 68 900 MPa. The axes of this figure are the initial outer gas volume radius, depth, and ratio of inner (shell) to outer (gas volume) radius. A noticeable ''rippling'' of the contours is evident in this figure, especially at higher shell thicknesses. To better isolate the effects at play causing this ''rippling,'' the maximum acoustic pressure is plotted versus

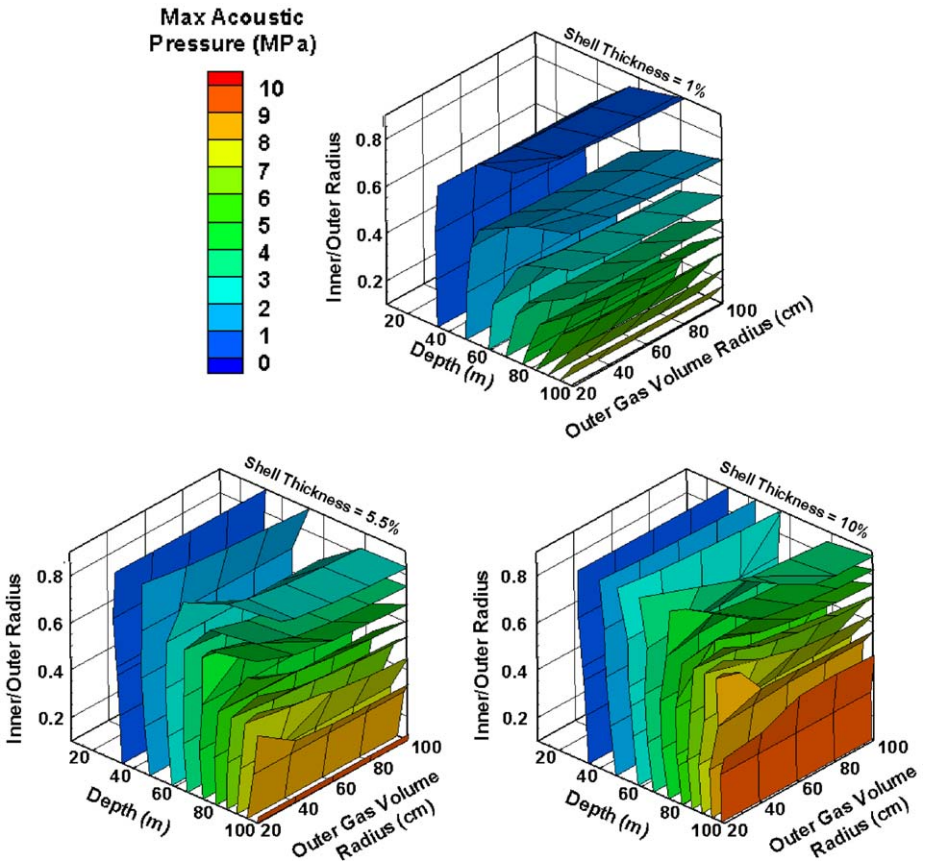


Fig. 20. Contour plots of maximum acoustic pressure at two times the initial outer volume radius with an elastic inner cylinder with a modulus of elasticity of 68 900 MPa.

depth and the ratio of inner-to-outer radius in Fig. 21. These data are plotted for an outer gas volume radius of 60 cm. The coloring in this figure is included to aid the eye in viewing the results. It can be seen that the maximum acoustic pressure peaks at the minimum inner-to-outer radius ratio. At the minimum value of this ratio, the maximum amount of gas volume is available to be compressed, and produce the maximum increase in pressure. Thus the "rippling" that is seen in Fig. 20 is actually caused by variation of the inner-to-outer radius ratio. It is also noted that the pressure always peaks at the minimum value of the inner-to-outer radius ratio in Fig. 20, while in the spherical volume study (Cor and Miller, 2009) the location of the peak pressure varied with the value chosen for the inner shell thickness.

### 4.3. Inner shells permitted to fail

Parametric studies were conducted with elastic and plastic inner shells that were allowed to fail. Trends were found to be very similar whether elastic or plastic inner shells were used. Therefore, the results of the plastic shell parametric study will be presented as representative of both cases. For this study, the material viscosity was 4000 N s/m$^2$, the material density was 7890 kg/m$^3$, the inner shell thickness was 10% and the plastic modulus was 345 MPa. Fig. 22 shows a contour plot for an initial outer gas volume radius of 60 cm. As before, the contours are for the maximum acoustic pressure encountered at two initial outer volume radii. In this figure, a phenomenon similar to what was seen in the spherical analysis is present once again: the maximum acoustic pressure appears to follow different "orbits" around points in depth/compressive failure stress-inner/outer radius space. The existence of these "orbits" can be explained in terms of work done on the inner shell. At a given depth, there is a failure stress at which the minimum acoustic energy is found. At failure stresses lower than this value, the acoustic energy rises because progressively less energy is absorbed by

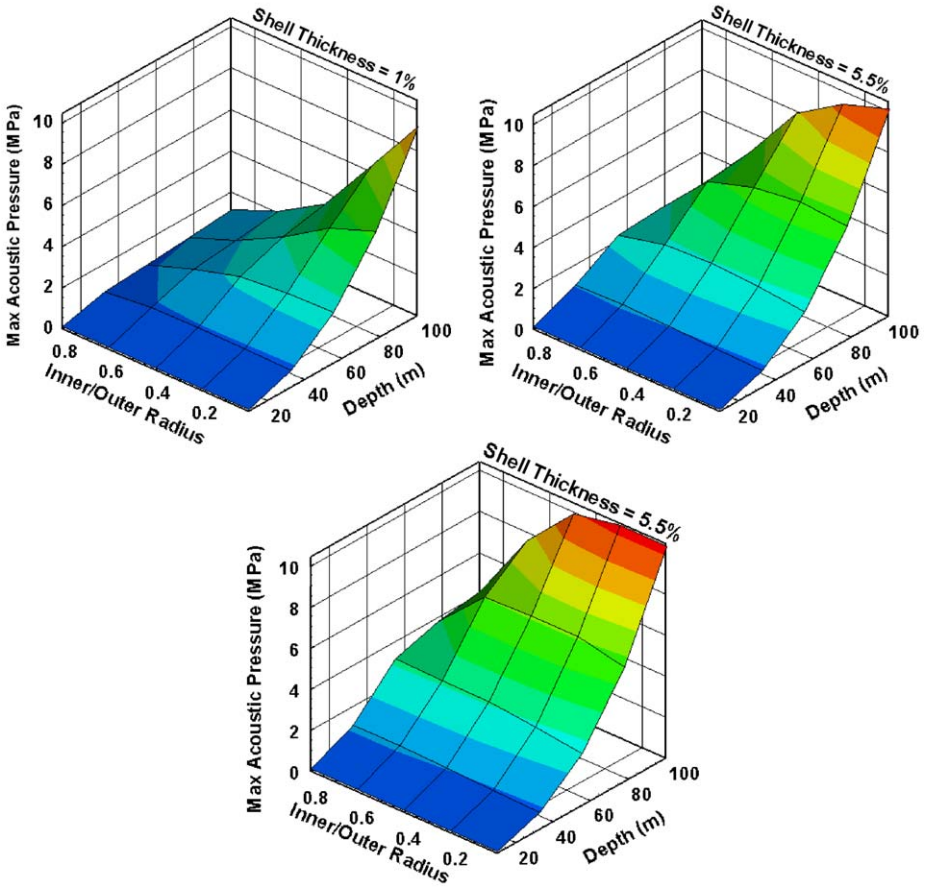


Fig. 21. Maximum acoustic pressure at two times the initial outer shell radius plotted against depth and the inner-to-outer radius ratio. The initial outer gas volume radius is 60 cm and the elastic modulus is 68 900 MPa.

the shell before it fails. As the failure stress is increased above this "saddle point" value, the growth in pressure inside the gaseous volume before failure tends to increase the maximum acoustic pressure.

## 5. Conclusions

Conditions for the various analyses in this study were chosen to be the same as in our previous work for spherical volumes to facilitate a direct comparison of the trends in spherical and cylindrical geometries. Comparable cylindrical geometries produced longer periods of oscillations with slightly smaller fluctuations in gas volume surface velocity and gas pressure. This can partially be explained by comparing the equations of motion for the two different geometries, and noting that for the spherical equation of motion (Eq. (3)) the gas pressure varies with the radius cubed, while for the cylindrical equation (Eq. (10) or Eq. (14)) the gas pressure varies with the radius squared. A given change in radius in the spherical case, therefore, will change the gas volume to a greater degree, which will tend to make the change in gas pressure larger. Another explanation for the higher gas velocities and pressures in the spherical cases is that the volume of water acting on the sphere in theory extends to infinity, while in the cylindrical case the assumption is that the influence only extends to a distance of 7.4 gas radii. This limits the hydrodynamic head that may build up in the cylindrical case. However, reviewing the results for the two geometries indicates that the differences in velocities and pressures are moderate. The effective ranges over which the implodable volume affects the liquid acoustic pressure were found to be comparable for the spherical and cylindrical cases. These results are another indication that the assumption of $\ln(r_0/R) = 2$ in the cylindrical case (Kedrinskii, 1976) is reasonable. Since a given change in radius creates a larger change

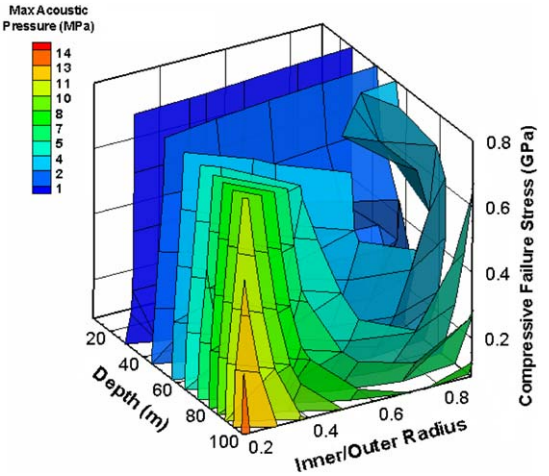


Fig. 22. Contour plots of maximum acoustic pressure at two times the initial outer volume radius with a plastic inner shell with a modulus of plasticity of 345 MPa, an inner shell thickness of 10%, and an initial outer gas volume radius of 60 cm.

in volume and gas pressure in the spherical case, the critical pressure that will negate the hydrodynamic head will be reached at a larger radius than in the cylindrical case. Thus the minimum radius of the gas volume is larger in the spherical case. This radius can also be achieved more quickly, producing larger oscillation frequencies in the spherical case.

When a brittle inner structure is present, it will tend to fail at a lower pressure for an imploding cylindrical volume than for an imploding spherical volume; however, the cylindrical volume's peak acoustic pressure is higher. This is because, for comparable radii, the relative volume left to be compressed after failure is less for the cylindrical case than for the spherical case. When the inner volume can deform plastically, the inner cylindrical structure will tend to deform to a greater degree than the spherical structure does, in part because of the higher hoop stress in the cylindrical case. This increased tendency of the inner structure to deform will lead to lower pressures in the outer gaseous volume and a lower acoustic pressure as well. When the inner structure can deform elastically, the cylindrical inner structure once again tends to deform to a greater degree than the spherical structure does, although the peak acoustic pressures for the cylindrical case is actually slightly higher. Overall trends found for spherical and cylindrical implodable volumes have been found to be very similar.

The analysis presented here and in Cor and Miller (2009) demonstrate once again that the existence of any interior structure inside the ruptured container, and its physical properties, can strongly reduce the strength of acoustic waves in the surrounding liquid. Therefore, we believe that these results demonstrate the advisability of revisiting the current safety criteria employed for imploding volumes with inner structures.

While trends for cylindrical and spherical geometries are similar, the findings for cylindrical geometries have a narrower range of applicability. They are most applicable for cylinders with large length-to-diameter ratios and at points nearly equidistant from the ends of the cylinder. Still, we believe that the simplified analysis presented here can be a useful tool for doing a computationally economical, first-order analysis on geometrical and structural effects on the pressure field produced when a cylindrical volume fails near a structure.

It is instructive to review some of the observations of Kedrinskii and co-workers in the context of our specific problem, and of our application of his methodology and equations. Kedrinskii and Kuzavov (1977) and Kedrinskii (2005) illustrate that the maximum radius and period of pulsation of a cylindrical cavity with detonation products is well approximated if the theoretical coefficient "3/4" is used in Eq. (5) with a constant value for $\gamma = 3$ in Kedrinskii (2005), or if this coefficient is set equal to unity and a variable $\gamma$ is used. Use of the unity value for the coefficient permits an analytical versus a numerical solution of Eq. (5). The theoretical coefficient (and consequently, numerical treatment) was employed here because the value of $\gamma$ for cases of interest is essentially constant (we are not interested in detonation events initiated by chemical explosives) and equal to that of an ideal gas. We prefer the use of "3/4" because it is justified by theory. Although the convenience of the analytic solution is attractive and offers physical insight for simpler configurations, interfacing the analytical solution with the numerical solution of the solid structures' behavior makes its ease of use less relevant.

Kedrinskii (1971) also observed that for an underwater explosion of a cylindrical charge, 80% of the energy of detonation products was radiated in the form of a shock wave. This and the supersonic velocities reported by Kedrinskii

(1972) for cylindrical underwater explosions suggests that the last term on the right hand side of Eq. (5)

$$(r/c)(1-v/c)\mathrm{d}w/\mathrm{d}t$$

should not be neglected. This suggestion appears to contradict the assumption made here that the surrounding water can be treated as essentially incompressible. The term $\mathrm{d}w/\mathrm{d}t$ represents the time rate of change of enthalpy; it is very large for chemically driven explosives, and is the reason for the production of a strong radiated shock wave. For an implosion initiated pressure pulse, the change in enthalpy is produced by recovery of the kinetic energy (dynamic pressure head) generated by the water accelerated into the cylindrical gas space by the difference between the external hydrostatic pressure head and the internal gas pressure. It is approximated by

$$\mathrm{d}w/\mathrm{d}t = u\,\mathrm{d}u/\mathrm{d}t$$

where $u$ is the maximum velocity of the cavity/water surface. The magnitude of this term is limited by the hydrostatic pressure (or depth) and the gas volume the water accelerates into. At not insignificant depths (such as those considered here) the magnitude of $\mathrm{d}w/\mathrm{d}t$ is nowhere near that produced by chemical explosives. This is illustrated in Fig. 4, which shows predictions of a maximum velocity of 100 m/s at 200 m depth, corresponding to an approximate Mach number $<0.1$. In short, at much greater depths than those dealt with here, the incompressible liquid assumption is not valid. However, for the work considered here, the last term on the right hand side of Eq.(5) may be neglected.

Finally, that the application of the approximation "$\ln(r_0/R) = 2$" in Eq. (12) gives good and reliable results for studies of two different types of problems (the implodable cylindrical cavity and the high speed supercavity) should not be too surprising in view of Kedrinskii's (2005) observation that the cavity formed near a liquid surface by an explosive charge has an analog in the cavity formed by a high-velocity penetration of a body into water (a class of problems also amenable to solution by supercavitation theory).

## Acknowledgement

The authors gratefully acknowledge the support of the Office of Naval Research under N00014-05-6-106 and administrator Dr Kam Ng.

## References

Cole, R.H., 1948. In: Underwater Explosions. Princeton University Press, Princeton.

Cor, J.J., Miller, T.F., 2009. Theoretical analysis of hydrostatic implodable volumes with solid inner structures. Journal of Fluids and Structures 25, 284–303.

Iakovlev, S., 2004. Influence of a rigid coaxial core on the stress–strain state of a submerged fluid-filled circular cylindrical shell subjected to a shock wave. Journal of Fluids and Structures 19, 957–984.

Iakovlev, S., 2006. Submerged fluid-filled cylindrical shell subjected to a shock wave: fluid–structure interaction effects. Journal of Fluids and Structures 23, 117–142.

Kalumuck, K.M., Duraiswami, R., Chahine, G.L., 1995. Bubble dynamics fluid–structure interaction simulation by coupling fluid BEM and structural FEM codes. Journal of Fluids and Structures 9, 861–888.

Kedrinskii, V.K., 1971. On oscillation of cylindrical gas cavity in boundless liquid, Continuum Dynamics. Institute of Hydrodynamics, SB of the USSR AS, Novosibirsk 8, 163–168.

Kedrinskii, V.K., 1972. Kirkwood–Bethe approximation for an underwater explosion with cylindrical symmetry. Combustion, Explosions and Shock Waves 8, 94–100.

Kedrinskii, V.K., 1976. Approximate models of one-dimensional pulsation of a cylindrical cavity in an incompressible fluid. Combustion, Explosions and Shock Waves 12, 768–773.

Kedrinskii, V.K., Kuzavov, V.T., 1977. Dynamics of cylindrical cavity in a compressible liquid. Journal of Applied Mechanics and Technical Physics 18, 515–519.

Kedrinskii, V.K., 2005. Hydrodynamics of Explosions, Experiments and Models. Springer Publishing, New York.

Klaseboer, E., Khoo, B.C., Hung, K.C., 2005. Dynamics of an oscillating bubble near a floating structure. Journal of Fluids and Structures 21, 395–412.

Lamb, H., 1932. In: Hydrodynamics. Dover Publications, New York.

Logvinovich, G.V., 1969. Hydrodynamics of Flows with Free Boundaries. NAUKOVA DUMKA, Kiev.

Likhterov, L., 2000. High-frequency acoustic emission generated by underwater explosion with cylindrical symmetry. ASME Journal of Fluids Engineering 122, 140–142.

Price, R.S., V.K. Shuler, 1974. Sounds from implosions of steel cylinders underwater. Naval Ordnance Laboratory Report NOLTR 74-168.

Rayleigh, L., 1917. On the pressure developed in a liquid during the collapse of a spherical cavity. Philosophical Magazine 34, 94–98.
Serebryakov, V.V., 1976. On one version of equations of principle ''cavity expansion independence''. Journal of Hydromechanics 34, 45–48.
Logvinovich, G.V., Serebryakov, V.V., 1975. On methods of calculating form of slender axisymmetric cavities. Journal of Gidromehanika 32, 47–54.
Tan, D., Sun, C., Yanping, W., 2003. Acceleration and viscoplastic deformation of spherical and cylindrical casings under explosive loading. Propellants, Explosives, and Pyrotechnics 28, 43–47.
Vokurka, K., 1985. On Rayleigh's model of a freely oscillating bubble. I. Basic relations. Czechoslovak Journal of Physics, B 35, 28–40.
Zong, Z., 2005. A hydroplastic analysis of a free–free beam floating on water subjected to an underwater bubble. Journal of Fluids and Structures 20, 359–372.